Shear Banding and Flow-Concentration Coupling in Colloidal Glasses

R. Besseling,[1] L. Isa,[1] P. Ballesta,[2] G. Petekidis,[2] M. E. Cates,[1] and W. C. K. Poon[1]

[1]*SUPA, School of Physics & Astronomy, The University of Edinburgh,*
Kings Buildings, Mayfield Road, Edinburgh EH9 3JZ, United Kingdom
[2]*IESL-FORTH and Department of Materials Science and Technology, University of Crete, Heraklion 71110, Crete, Greece*

We report experiments on hard-sphere colloidal glasses that show a type of shear banding hitherto unobserved in soft glasses. We present a scenario that relates this to an instability due to shear-concentration coupling, a mechanism previously thought unimportant in these materials. Below a characteristic shear rate $\dot{\gamma}_c$ we observe increasingly nonlinear and localized velocity profiles. We attribute this to very slight concentration gradients in the unstable flow regime. A simple model accounts for both the observed increase of $\dot{\gamma}_c$ with concentration, and the fluctuations in the flow.

Shear banding is widespread in the flow of disordered materials, including complex fluids [1], pastes, gels, and emulsions [2], granular matter [3], soils and rocks [4], and metallic glasses [5]. Understanding this phenomenon is thus crucial in various fields of science and engineering.

Constitutive models of shear banding exist, e.g., in wormlike micellar fluids [1], where a flow curve of stress versus strain rate $\sigma(\dot{\gamma})$ with slope $\eta_d < 0$ causes instability and separation into two bands with distinct flow rates $(\dot{\gamma}_1, \dot{\gamma}_2) > 0$ [1]; these can also have distinct concentrations [6]. Many systems with a yield stress ($\sigma_y > 0$) also show coexistence of distinct bands [7–10], with one band now being solid ($\dot{\gamma}_1 = 0$). In some cases this stems from a similar mechanical instability ($\eta_d < 0$ for $\dot{\gamma} < \dot{\gamma}_2$) [9–12] due to positive feedback between flow and structural breakup. However, the banding seen in other experiments [13–16] and simulations [17,18] cannot be explained in those terms, particularly for purely repulsive interactions [19]. In some of these systems, banding may be attributed to cooperativity between local plastic events, characterized by a cooperativity length ξ. However, theory [20] and simulations [21] show that ξ grows when the flow slows down, which contrasts with the rate independence seen in experiments [15].

In this Letter we show by experiment and theory that concentrated hard-sphere (HS) colloids, one of the simplest yield-stress fluids and a model for soft glasses generally, can exhibit a type of shear banding that does not fit into any of the above categories. Instead, we propose a scenario where banding is caused by shear-concentration coupling (SCC). Though well known as a generic mechanism for flow instability [22], this has not previously been explored as a shear-banding mechanism in glasses. This is perhaps because the concentration changes involved can be extremely small, as we show below; hence they are not directly detectable in experiments. Crucially, the effects on flow of very small concentration gradients are vastly amplified by the presence of a yield stress.

It is well known that for *nonuniform* stress, particle migration [23] is driven by gradients in $\dot{\gamma}$ and the nonequilibrium particle pressure, $\Pi(\dot{\gamma})$ [24,25]. The resulting concentration inhomogeneity causes departures from flow profiles for the homogeneous system. But this cannot explain such departures under *uniform* stress, which requires *intrinsic* instability [22] (see also [23]). Recent theories [26] show that Newtonian and linearly viscoelastic materials can also exhibit such instability via SCC. However, this arises at 45° to the flow direction, and is unrelated to the results in [22] on SCC-induced instability in *nonlinear* fluids. In applying the latter to glasses, our two key ingredients are (nonlinear) dilatancy (the tendency of jammed systems to expand under flow, $\partial\Pi/\partial\dot{\gamma} > 0$) and flow nonlinearity. As both are ubiquitous in glassy materials, our results are likely to have wide relevance.

We used sterically stabilized polymethylmethacrylate particles (radii $a = 138$ nm and 150 nm, polydispersity $\sim 15\%$) suspended in a decalin-tetralin mixture (viscosity $\eta_s = 2.3$ mPa s) and seeded with $\sim 0.5\%$ fluorescent colloids ($a = 652$ nm) of the same kind. Different volume fractions ϕ were prepared by diluting samples centrifuged to a sediment with $\phi = \phi_m \simeq 0.67$; we report data in terms of the reduced concentration $\Phi = \phi/\phi_m$. The glass transition was found to lie at $\Phi_g \simeq 0.86$ [27].

Rheology was measured in an AR2000 rheometer in cone and transparent plate geometry (cone angle 1°, radius 20 mm), coupled to a confocal microscope [28,29] to measure the velocity $v(z)$ across the gap, $0 \le z \le z_g$, at various z_g. For $\dot{\gamma} \gtrsim 0.1$ s^{-1} we measured $v(z)$ at each z for a time $\ge 3/\dot{\gamma}$; for $\dot{\gamma} \lesssim 0.1$ s^{-1}, $v(z)$ was measured from rapid 3D scans [29] over a time $\sim 2/\dot{\gamma}$. The reported $v(z)$ are constant over the measurement time. To prevent slip [28], walls were coated with a disordered monolayer of the tracers; results for a cone and/or plate roughened to ~ 10 μm were very similar. We took data at fixed $\dot{\gamma}$, stepping down $\dot{\gamma}$ after 300 s preshear at $\dot{\gamma} \simeq 10$–30 s^{-1} or stepping up from $\dot{\gamma} = 0$ (waiting for $\ge 2/\dot{\gamma}$ before acquiring $v(z)$ in either case).

The results showed no systematic differences between these protocols; stress-controlled measurements also showed no significant changes.

For $\Phi \gtrsim \Phi_g$, the bulk rheology is as previously reported, Fig. 1(a), with flow curves of Herschel-Bulkley (HB) form: $\sigma - \sigma_y \propto \dot{\gamma}^n$, with $n \simeq 0.4$–0.5. The strong increase of σ_y with Φ, due to the vanishing of free volume as $\Phi \to 1$ [30], is consistent with $\sigma_y(\Phi) \simeq \sigma_0(1 - \Phi)^{-p}$ with $p \simeq 3$ and $\sigma_0 \simeq 0.01 k_B T/a^3$, Fig. 1(b).

Until now, HB and similar monotonic flow curves for glasses have not been linked to nontransient shear banding. However, the underlying velocity profiles, shown in Fig. 1(c) for $z_g = 170 \ \mu$m and $\Phi = 0.933$, exhibit a marked change when we decrease the imposed shear rate $\dot{\gamma} = \int \dot{\gamma}(z)dz/z_g$ (here $\dot{\gamma}(z) \equiv \partial_z v$). At large $\dot{\gamma}$, $v(z)$ is linear, but for $\dot{\gamma} = 0.2 \ \mathrm{s}^{-1}$ $v(z)$ becomes highly nonlinear, with an enhanced rate near the plate and a progressive reduction towards the cone. For even smaller rates, $\dot{\gamma} \lesssim 0.05 \ \mathrm{s}^{-1}$, the nonlinearity grows and $\dot{\gamma}(z)$ decreases *continuously* from a value $\gg \dot{\gamma}$ near the plate to $\dot{\gamma}(z) \simeq 0$ for larger z. The width of the fluidized band appears to saturate for low $\dot{\gamma}$ at $\sim 80a$ (not shown); we find no evidence for a minimum strain rate in this band [31]. The behavior for $z_g = 60 \ \mu$m and $90 \ \mu$m is essentially the same. Such continuously varying flow profiles strongly contrast with the distinct solid and fluid bands in thixotropic yield-stress fluids [9,10]. HS glasses, which show only very weak aging of quiescent properties [30], are thus distinct from such systems. Note from Figs. 1(c) and 2(b) that $v(z)$ has no unique "symmetry": the fluidized band may appear near either the plate or

the cone. This rules out sedimentation or specific wall rheology [15] as explanations [32]. The growth of the fluidized band with $\dot{\gamma}$ also contrasts with the rate dependence (or lack thereof) of the cooperativity length found in [15,20].

Next, we discuss the concentration dependence of the observed behavior, Fig. 2. For both $\Phi = 0.895$ [just within the glass, Fig. 2(a)] and for a much higher concentration $\Phi = 0.948$, Fig. 2(b), we again observe a transition to a nonlinear velocity profile as $\dot{\gamma}$ is lowered, but the shear rate at which this occurs is, respectively, much smaller and higher than for $\Phi = 0.933$, Fig. 1(c). On decreasing $\dot{\gamma}$, we define the critical shear rate, $\dot{\gamma}_c$, to be that point at which the maximum deviation from linearity of the normalized velocity profile, $|v(z) - \dot{\gamma}z|/v_{\mathrm{cone}}$, first exceeds 0.1. Results for the critical Péclet number, $\mathrm{Pe}_c = \dot{\gamma}_c \tau_B$ (where $\tau_B = 6\pi\eta_s a^3/k_B T$ is the Brownian time) are shown as a function of Φ in Fig. 3.

To begin to interpret our observations, we first show that the observed velocity profiles can be reconciled with HB behavior, simply by postulating a small concentration variation $\delta\Phi(z)$ across the gap. Writing the HB form as $\dot{\gamma}\tau = [(\sigma/\sigma_y(\Phi)) - 1]^{1/n}$ with $\sigma_y(\Phi) = \sigma_0(1 - \Phi)^{-3}$ as before, we can then calculate $v(z, \sigma) = \int_0^z \dot{\gamma}(\bar{\Phi} + \delta\Phi(z'), \sigma)dz'$ for a given mean concentration $\bar{\Phi}$ and a choice of $\delta\Phi(z)$. In Fig. 4(a) we do this for a uniform gradient $\partial\delta\Phi(z)/\partial z = |\delta\Phi|/z_g$ with $|\delta\Phi|/\bar{\Phi} = 0.002$, at various values of the reduced stress $\sigma/\sigma_y(\bar{\Phi})$. When σ approaches $\sigma_y(\bar{\Phi})$, $v(z)$ changes from weakly to strongly nonlinear, reflecting the progressive localization of shear within regions of the sample with the lowest yield stress $\sigma_y(\Phi(z))$, i.e., with the lowest $\Phi(z)$. These results strikingly resemble the experimental data in Fig. 1(b), although $\delta\Phi$ is too small to be directly measured [33]; different symmetries of $v(z)$ in other experiments can also be explained by corresponding changes in $\delta\Phi(z)$. Note that the mean shear rate $\dot{\gamma} = v(z_g, \sigma, \Phi(z))/z_g$ differs from $\dot{\gamma}(\sigma, \bar{\Phi})$, but the *effective* flow curves $\sigma(\dot{\gamma}, \Phi(z))$ deviate only slightly from the uniform $\sigma(\dot{\gamma}, \bar{\Phi})$; see Fig. 4(b).

While concentration gradients can thus account for the results, their origin and the enhanced shear localization with increasing $\bar{\Phi}$ remain to be explained. We now show that both are explicable via the SCC instability scenario of [22]. Fluctuations in concentration ($\delta\Phi$) and shear rate
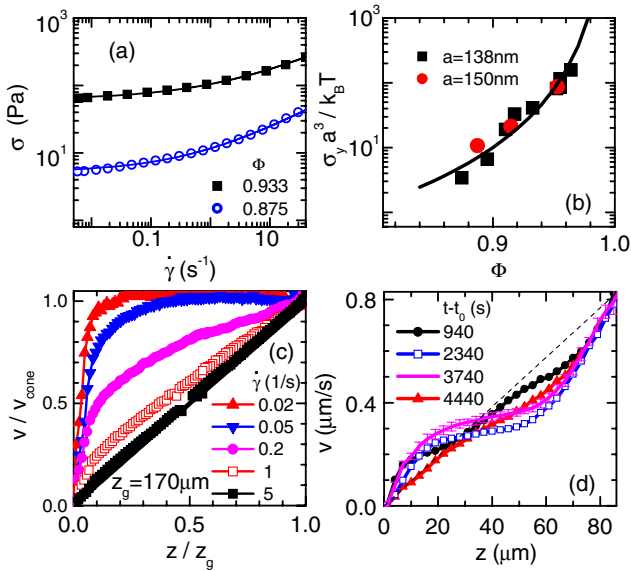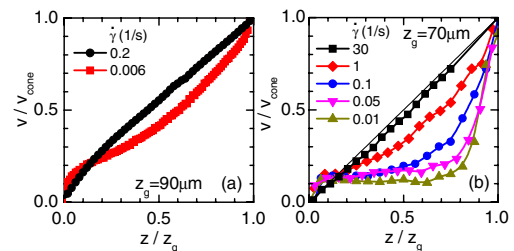

FIG. 1 (color online). (a) Flow curves $\sigma(\dot{\gamma})$ with HB fits (lines) for $\Phi = 0.875$ and $\Phi = 0.933$. (b) Yield stress versus Φ. Line: $\sigma_y = \sigma_0(1 - \Phi)^{-3}$ with $\sigma_0 = 0.01 k_B T/a^3$. (c) Velocity profiles $v(z)$ for $\Phi = 0.933$ at various $\dot{\gamma}$. (d) Evolution of $v(z)$ after startup shear of $\dot{\gamma} = 0.01 \ \mathrm{s}^{-1}$ at t_0 ($\Phi = 0.94$); data for $t - t_0 = 3740$ s show error bars. Data in (a),(c) and (d) are for $a = 138$ nm.

FIG. 2 (color online). Velocity profiles at different Φ: (a) $\Phi = 0.895$ ($a = 138$ nm), (b) $\Phi = 0.948$ ($a = 150$ nm).
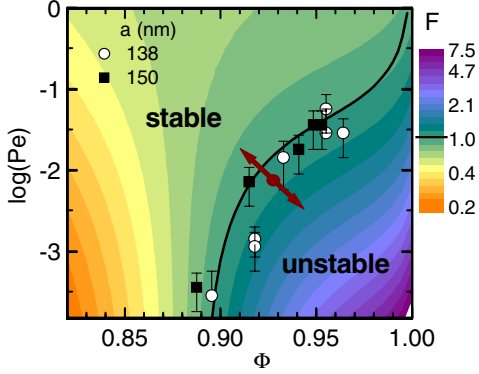
FIG. 3 (color online). Line: critical flow rate $Pe_c(\Phi)$ from
Eq. (7) with $[p, r, m = n, A, B] = [3, 4, 0.4, 25, 0.005]$. Colors
mark the value of F. Symbols: experimental values for Pe_c
(averaged over z_g). Arrow: possible evolution of an unstable state.

$(\delta\dot{\gamma})$ evolve via the diffusion and Navier-Stokes equations,
in which shear-induced migration and the Φ dependence of
the shear stress must be included [22]. For small fluctua-
tions along z we have (to linear order in $\delta\Phi$, $\delta\dot{\gamma}$):

$$\partial_t \delta\Phi = -\vec{\nabla} \cdot \vec{J} \simeq M(\Pi_\Phi \partial_z^2 \delta\Phi + \Pi_{\dot{\gamma}} \partial_z^2 \delta\dot{\gamma}), \quad (1)$$

$$\partial_t \delta\dot{\gamma} = \rho^{-1}\partial_z^2 \sigma \simeq \rho^{-1}(\sigma_\Phi \partial_z^2 \delta\Phi + \sigma_{\dot{\gamma}} \partial_z^2 \delta\dot{\gamma}). \quad (2)$$

Here we have introduced the shorthand $\Pi_{\dot{\gamma}} \equiv \partial\Pi/\partial\dot{\gamma}|_\Phi$,
likewise Π_Φ, $\sigma_{\dot{\gamma}}$ and σ_Φ; M is a collective mobility and ρ
the density. The migration current $\vec{J}$ arises from particle
pressure gradients $\partial_z \Pi(\Phi, \dot{\gamma})$ due to variations in both Φ
and $\dot{\gamma}$ [24,35]. The terms involving $\Pi_{\dot{\gamma}}$ and σ_Φ in Eqs. (1)
and (2) cause, respectively, particle migration towards
regions of low shear rate, and accelerated shear in regions
of low concentration; together, these amplify fluctuations.
That is, a fluctuation towards higher Φ in some region
creates a lower shear rate there. This promotes inward
particle migration, giving a positive feedback effect. This
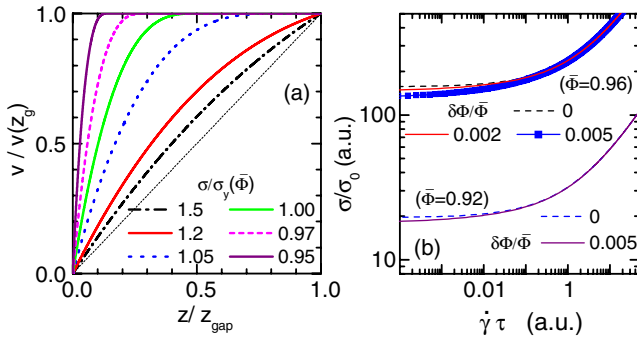tendency is counteracted by the remaining terms which

FIG. 4 (color online). Velocity profiles $v(z)/v(z_g)$, calculated
from $\dot{\gamma} \propto [(\sigma/\sigma_y[\Phi(z)]) - 1]^2$ and $\sigma_y \propto (1 - \Phi)^{-3}$, with
$\Phi(z) - \bar{\Phi} = |\delta\Phi|[(z/z_g) - (1/2)]$ with $\bar{\Phi} = 0.96$, $|\delta\Phi|/\bar{\Phi} =$
0.002, for different $\sigma/\sigma_y(\bar{\Phi})$. (b) Effective flow curves σ versus
$\dot{\gamma} = v(z_g, \sigma, \Phi(z))/z_g$ for various $\bar{\Phi}$ and $|\delta\Phi|$.

describe stable diffusive spreading of both particles and
momentum (or equivalently shear rate). Rewriting Eqs. (1)
and (2) as $\partial_t \Psi_i = L_{ij}\partial_z^2 \Psi_j$ with $\Psi_i = (\delta\Phi, \delta\dot{\gamma})$, we see
that instability sets in when $\det L_{ij} = M(\Pi_\Phi \sigma_{\dot{\gamma}} -$
$\Pi_{\dot{\gamma}}\sigma_\Phi)/\rho$ becomes negative, or equivalently, as first
derived in [22,35], when

$$F \equiv \frac{\Pi_{\dot{\gamma}}\sigma_\Phi}{\Pi_\Phi \sigma_{\dot{\gamma}}} > 1. \quad (3)$$

To evaluate F, we first write the HB form for σ in terms of
the Péclet number $Pe = \dot{\gamma}\tau_B$:

$$\sigma = \frac{\sigma_0}{(1 - \Phi)^p}[1 + s(\Phi)Pe^n], \quad s(\Phi) = A(1 - \Phi)^n. \quad (4)$$

The first term is σ_y and $n \simeq 0.4$–0.5, as before. Typical
values for A from our experiments are $A = 10$–20. The
particle pressure Π for HS colloids has a similar form:

$$\Pi = \frac{\Pi_0 \Phi}{(1 - \Phi)}[1 + g(\Phi)Pe^m], \quad g(\Phi) \equiv B(1 - \Phi)^{1-r}. \quad (5)$$

Here, $\Pi_0 = 2.175\phi_m k_B T/\pi a^3$; the first term then approx-
imates the osmotic pressure at rest [36], the second term is
the contribution due to shear. For the latter, a Pe^2 depen-
dence was found in [36,37], but this is restricted to a
linearly viscous regime ($\sigma \propto Pe$) at very small Pe, in which
Eq. (3) yields $F \propto Pe^2$ resulting in stable flow. However,
this regime is hard to access, and indeed completely absent
when σ_y is nonzero ($\Phi > \Phi_g$), where it is replaced by a
non-Newtonian regime in which both σ and Π increase
sublinearly with Pe. From simulations for $\Phi \lesssim \Phi_g$ [24,37],
we extract $m = 0.4$–0.5, (and $B \simeq 0.003$, $r \simeq 3$), so that
$m \simeq n$, as also seen in simulations of 2D foams [38]. For
$\Phi \gtrsim \Phi_g$, and for glassy flow in general, we expect m and
n to remain similar (e.g., within mode coupling theory,
$m = n$ seems probable [19]).

Using Eqs. (4) and (5), we obtain a limiting value for F
at large Pe as $F_\infty = m(p - n)/nr$. The flow is thus stable
in this regime provided $r > p - n$; to explain our experi-
ments we require $r \gtrsim 2.5$. More interesting is the result for
small Pe, where we obtain

$$F \to Pe^{m-n}\frac{mpg(\Phi)\Phi}{ns(\Phi)} \simeq \frac{mpB\Phi}{nA(1 - \Phi)^{r+n-1}} = F_0. \quad (6)$$

Here, $F_0(\Phi)$ is a quasiplateau value maintained while
$Pe^{m-n} \simeq 1$ (and a true limiting value if $m = n$). It follows
that homogeneous flow at low Pe is *unstable* for concen-
trations $\Phi > \Phi_c$, where $F_0(\Phi_c) = 1$. We argue that it is
this SCC-induced instability that creates the small varia-
tions $\delta\Phi(z)$ that were assumed in Fig. 4(a), and which
account for the experimentally observed localized flow at
small $\dot{\gamma}$. Because, as in [22], our analysis is limited to
linear stability, we do not have a clear idea of the mecha-
nism limiting the growth of $\delta\Phi$. However, the extreme
nonlinear dependence of both σ and Π on Φ as $\Phi \to 1$
makes it plausible that $\delta\Phi$ remains small.

The critical flow rate Pe_c, below which the instability sets in, follows from $F(Pe_c, \Phi) = 1$. For $m = n$ this gives

$$Pe_c(\Phi) \simeq \left[\frac{p}{rs(\Phi)(1 - F_\infty)} \left(1 - \frac{1}{F_0(\Phi)} \right) \right]^{1/n}. \quad (7)$$

Figure 3 shows $Pe_c(\Phi)$ for specific parameter values. Entering the unstable regime $\Phi > \Phi_c$, Pe_c increases and grows $\sim s(\Phi)^{-1/n}$ for $\Phi \to 1$. Our model provides a quantitative account of the data; the fit [39] gives $\Phi_c = 0.89$, close to, but above, Φ_g. In contrast to most shear-banding scenarios [1], the present system seems unable to achieve global stability by separating into distinct bands. This is shown by the arrows in Fig. 3: an initially unstable state can form a locally depleted region, $\Phi(z) < \bar{\Phi}$, that is stabilized when $Pe(\Phi(z)) > Pe_c$, but the remaining concentrated region becomes even more unstable. This suggests that the banded flow should have residual temporal fluctuations. We have indeed observed this [Fig. 1(d)]; after startup shear of $\dot{\gamma} = 0.01$ s^{-1}, a weakly nonlinear profile develops a central region where $\dot{\gamma}(z)$ is strongly reduced, which then speeds up by expanding the lower band, and subsequently reverts to a larger $\dot{\gamma}(z)$. We have also observed (in a planar shear cell [31]) that a fluidized band can swap from $z \simeq 0$ to $z \simeq z_g$ over sufficient time. Leaving a detailed study of these effects for future work, we note that the shear-banding we observe is permanent (if unsteady) not transient; moreover, our stress is time-independent, in contrast to the results in [16].

Our shear-banding arises from the Φ dependent nonlinear rheology of glasses along with the nonlinear process of "Brownian dilation" whereby flow increases the particle pressure $\Pi(\Phi, Pe)$. For larger Pe than those studied here, hydrodynamic effects cause a much stronger increase of Π with Pe [25], ultimately leading to shear thickening in these suspensions. Hence, the localization we observe might be interpretable as a precursor to thickening.

In conclusion, we have shown that HS colloidal glasses exhibit a new type of shear banding, well described by a model in which SCC leads to unstable flow near yielding. In this scenario, very small concentration variations can sustain large variations in flow rate. Our results may also be relevant for flow in other glassy materials, such as foams where dilatancy has recently been observed [40]. It may also shed light on shear bands and dilatancy in metallic glasses [5]. We mention in particular simulations of a model glass [17], which showed both fluctuating shear bands and small but finite concentration gradients.

[1] M. E. Cates and S. M. Fielding, Adv. Phys. **55**, 799 (2006); P. D. Olmsted, Rheol. Acta **47**, 283 (2008); J. K. G. Dhont and W. J. Briels, Rheol. Acta **47**, 257 (2008).
[2] G. Ovarlez et al., Rheol. Acta **48**, 831 (2009).
[3] H. M. Jaeger et al., Rev. Mod. Phys. **68**, 1259 (1996).
[4] J. W. Rudnicki, J. Mech. Phys. Solids **23**, 371 (1975).
[5] F. Spaepen, Acta Metall. **25**, 407 (1977); **30**, 447 (1982); J. Li et al., Philos. Mag. A **82**, 2623 (2002).
[6] S. M. Fielding and P. D. Olmsted, Eur. Phys. J. E **11**, 65 (2003); M. E. Helgeson et al., Phys. Rev. Lett. **105**, 084501 (2010).
[7] P. Coussot et al., Phys. Rev. Lett. **88**, 218301 (2002).
[8] S. A. Rogers, D. Vlassopoulos, and P. T. Callaghan, Phys. Rev. Lett. **100**, 128304 (2008).
[9] P. Moller et al., Phys. Rev. E **77**, 041507 (2008).
[10] V. Bertola et al., J. Rheol. **47**, 1211 (2003).
[11] G. Picard et al., Phys. Rev. E **66**, 051501 (2002); S. M. Fielding et al., Soft Matter **5**, 2378 (2009).
[12] P. Coussot et al., Phys. Rev. Lett. **88**, 175501 (2002).
[13] T. G. Mason et al., J. Colloid Interface Sci. **179**, 439 (1996); F. Rouyer et al., Phys. Rev. E **67**, 021405 (2003); L. Becu, S. Manneville, and A. Colin, Phys. Rev. Lett. **96**, 138302 (2006); see also [34].
[14] G. Katgert et al., Europhys. Lett. **90**, 54002 (2010).
[15] J. Goyon et al., Nature (London) **454**, 84 (2008).
[16] T. Divoux et al., Phys. Rev. Lett. **104**, 208301 (2010).
[17] F. Varnik et al., Phys. Rev. Lett. **90**, 095702 (2003).
[18] Y. Shi et al., Phys. Rev. Lett. **98**, 185505 (2007).
[19] J. M. Brader et al., Proc. Natl. Acad. Sci. U.S.A., **106**, 15 186 (2009).
[20] L. Bocquet, A. Colin, and A. Ajdari, Phys. Rev. Lett. **103**, 036001 (2009).
[21] R. Yamamoto and A. Onuki, Phys. Rev. E **58**, 3515 (1998); G. Picard et al., Phys. Rev. E **71**, 010501 (2005).
[22] V. Schmitt, C. M. Marques, and F. Lequeux, Phys. Rev. E **52**, 4009 (1995).
[23] P. R. Nott and J. F. Brady, J. Fluid Mech. **275**, 157 (1994).
[24] Y. Yurkovetsky and J. F. Morris, J. Rheol. **52**, 141 (2008).
[25] A. Deboeuf et al., Phys. Rev. Lett. **102**, 108301 (2009).
[26] A. Furukawa and H. Tanaka, Nature (London) **443**, 434 (2006); Nature Mater. **8**, 601 (2009).
[27] W. van Megen et al., Phys. Rev. E **58**, 6073 (1998).
[28] P. Ballesta et al., Phys. Rev. Lett. **101**, 258301 (2008).
[29] R. Besseling et al., Adv. Colloid Interface Sci. **146**, 1 (2009).
[30] N. Koumakis et al., Soft Matter **4**, 2008 (2008); K. S. Schweizer and G. Yatsenko, J. Chem. Phys. **127**, 164505 (2007).
[31] R. Besseling et al., Phys. Rev. Lett. **99**, 028301 (2007).
[32] In our geometry $\sigma(z)$ is uniform within 0.03%.
[33] Typically $\delta\phi \lesssim 0.3\%$ suffices, below our imaging resolution ($\gtrsim 0.5\%$). MRI experiments [34] may detect this.
[34] G. Ovarlez et al., Phys. Rev. E **78**, 036307 (2008).
[35] In [22], J was described via a chemical potential $\mu(\Phi, \dot{\gamma})$. Here we use $J = -M[\partial_\Phi \Pi \nabla \Phi + \partial_{\dot{\gamma}} \Pi \nabla \dot{\gamma}]$ as in [24,25].
[36] J. F. Brady and M. Vicic, J. Rheol. **39**, 545 (1995).
[37] R. Foss and J. F. Brady, J. Rheol. **44**, 629 (2000).
[38] V. J. Langlois, S. Hutzler, and D. Weaire, Phys. Rev. E **78**, 021401 (2008).
[39] In the fit we fix $p = 3$, $m = n$, and vary A, B, n, and r.
[40] S. P. L. Marze et al., Colloids Surf. A **263**, 121 (2005).